Proton removal from ^{8}B, ^{9}C, and ^{12}C on Si at 20–70 MeV/nucleon

R. E. Warner,[1] F. D. Becchetti,[2] J. A. Brown,[3] A. Galonsky,[4] J. H. Kelley,[5] A. Nadasen,[6] R. M. Ronningen,[4] J. A. Tostevin,[7] J. S. Winfield,[4,*] and P. Zecher[4,†]

[1]*Oberlin College, Oberlin, Ohio 44074, USA*
[2]*University of Michigan, Ann Arbor, Michigan 48109, USA*
[3]*Wabash College, Crawfordsville, Indiana 47933, USA*
[4]*National Superconducting Cyclotron Laboratory, East Lansing, Michigan 48824, USA*
[5]*Triangle Universities Nuclear Laboratory, Durham, North Carolina 27706, USA*
[6]*University of Michigan, Dearborn, Michigan 48128, USA*
[7]*Department of Physics, School of Electronics and Physical Sciences, University of Surrey, Guildford, Surrey GU2 7XH, United Kingdom*

(Received 22 May 2003; revised manuscript received 20 November 2003; published 26 February 2004)

A Si detector telescope, in which alternating thick and thin Si elements served as both targets and detectors, was used to measure the energy dependence of the inclusive one-proton-removal cross sections σ_{1p} of ^{8}B, ^{9}C, and ^{12}C on a Si target. A similar detector telescope was used to measure both σ_{1p} and σ_{2p} for ^{9}C; σ_{2p} of ^{9}C is more than twice as large as σ_{1p} of ^{9}C and almost as large as σ_{1p} of ^{8}B. The measurements were compared with shell model calculations using eikonal reaction theory. The quenching factors R_s (the ratio of the measurement to the theoretical prediction) for ^{8}B and ^{9}C were near unity, as at higher energies. They also agreed with those measured recently for those nuclei on a C target at 75 MeV/nucleon. For ^{12}C the quenching is greater with $R_s = 0.44 \pm 0.03$. This is comparable to the value 0.53 ± 0.02 deduced at energies above 1 GeV/nucleon.

DOI: 10.1103/PhysRevC.69.024612 PACS number(s): 24.10.−i, 25.60.Gc, 25.70.Mn

I. INTRODUCTION

Controversy continues over whether ^{8}B is a proton-halo nucleus. Several pieces of evidence—including its large quadrupole moment [1], enhanced reaction cross sections σ_R at sub-Coulomb [2] and medium bombarding energies [3,4], momentum distributions of the ^{7}Be fragments following breakup [5,6], and the asymptotic normalization coefficient (ANC) for proton transfer in the peripheral (^{7}Be,^{8}B) reaction [7]—argue for such a halo. Moreover, proton-removal measurements at relativistic energies [8] quantify the excited core component in the ^{8}B ground-state wave function and establish the dominance of the $1p$ proton configuration. However, the lack of enhancement in the high-energy interaction cross sections σ_I [9] argues against a halo. Furthermore, polarization of the ^{7}Be core can enhance the ^{8}B quadrupole moment [10], while the ^{7}Be fragment momentum distributions are modified by the reaction mechanism and therefore do not directly measure the valence proton momentum-space wave function [11].

Nucleon-removal cross sections, σ_{1p} in the case of ^{8}B, are important for an understanding of the structure of halo nuclei since they are sensitive to details of the single-particle wave function in the nuclear surface [12]. In contrast, contributions to σ_R and σ_I come from the many-body wave function throughout the entire nuclear volume, and are less sensitive to the halo-defining surface region. This paper reports σ_{1p} data for 20–60 MeV/nucleon ^{8}B projectiles incident on a Si target. These data are compared with two older inclusive data sets [4,13] and with the predictions of the shell model by the use of an effective three-body reaction model [14,15]. Our data span a larger energy range than the older data and thus test more effectively the predicted energy dependence. The new data result from additional analysis of earlier measurements [3] of σ_R for ^{8}B on Si. We show that the Si target-detector telescope of that experiment—hereafter called Experiment 1—also is well suited to measuring the energy dependence of σ_{1p} for light projectiles at bombarding energies up to about 70 MeV/nucleon.

There are few available data for the nucleus ^{9}C. Its unusually small $2p$-separation energy (1.43 MeV) is only slightly larger than that of ^{17}Ne(0.94 MeV) which has been proposed as a $2p$-halo nucleus because of its anomalously large σ_I at high energy [16]. Single-proton removal from ^{9}C leaves the weakly bound nucleus ^{8}B, in contrast to ^{17}Ne which would be left as the unbound nucleus ^{16}F. The σ_{xp} of ^{9}C are therefore possible indicators of its structure. An interesting aspect of nucleon removal is that, when single-nucleon removal leaves a halo or other weakly bound nucleus, the cross section for removing two nucleons can exceed that for removing only one nucleon. This effect was observed for neutron removal from ^{12}Be at 50 MeV/nucleon [17] and proton removal from ^{9}C at 75 MeV/nucleon [18] and at 285 MeV/nucleon [19]. Finally, the small binding energy of the last proton allows the astrophysically important ANC for the $p+^{8}$B system to be extracted from proton-removal data [20]. We report here values of σ_{1p} and σ_{2p} for 30–50 MeV/nucleon ^{9}C on Si. These were obtained from a later experiment [21]—hereafter called Experiment 2—which also employed a Si telescope for σ_R measurements.

*Present address: INFN-LNS, Via S. Sofia 44, 95123 Catania, Italy.
†Present address: Investor Analytics LLC, 80 Broad Street, New York, NY 10004.

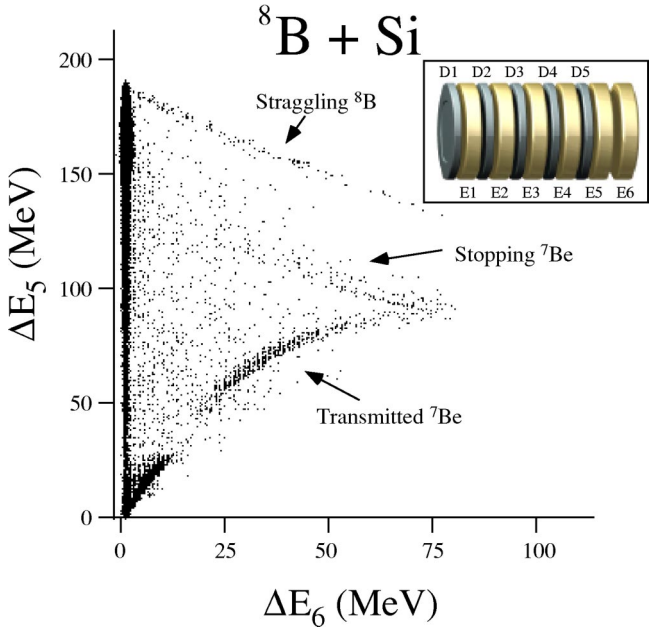

FIG. 1. A scatter plot for the last two elements of the Si target-detector telescope (shown in inset) used in Experiment 1. The incident secondary beam is 62 MeV/nucleon ^{8}B.

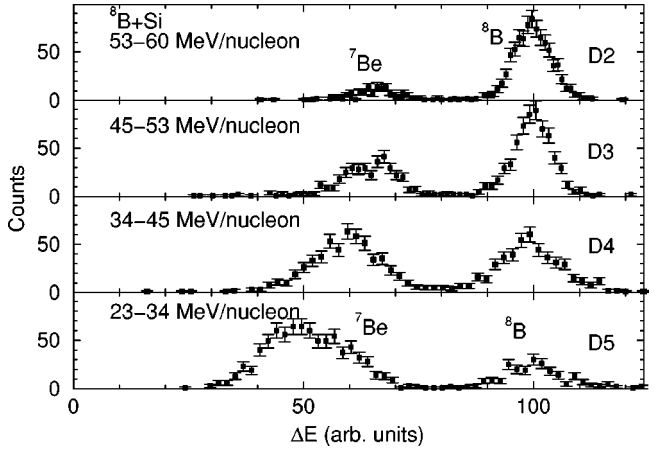

FIG. 2. Energy loss spectra in four thin detectors (see Fig. 1) from incident ^{8}B, gated on the ^{7}Be fragments identified in detectors E5 and E6.

Finally, we present σ_{1p} data for ^{12}C on Si. This well-bound nucleus is interesting to contrast with ^{8}B since, at energies above 200 MeV/nucleon, the measured values of σ_{1p} for ^{12}C are only about half those predicted using the shell model and eikonal reaction theory [22]. Similar reductions, or quenching of the predicted shell model single-particle strength, have been observed in analyses of $(e,e'p)$ knockout reaction data.

II. EXPERIMENTAL METHOD

The measurements of Experiment 1, for ^{8}B, ^{9}C, and ^{12}C on Si, are described in this Section. A brief summary of Experiment 2, which produced most of our ^{9}C data, is included in Sec. III.

The three projectiles used in this study were produced as secondary beams by fragmentation of a primary 80 MeV/nucleon ^{18}O beam at the National Superconducting Cyclotron Laboratory. The targets for the primary beam were 0.5 g/cm^2 Be for ^{8}B and ^{9}C, and 0.6 g/cm^2 C for ^{12}C. Both ^{8}B and ^{9}C were components of a compound secondary beam which initially contained about 70% ^{7}Be and little ^{9}C; later adjustment of the magnetic analyzing system not only decreased the ^{7}Be content to about 20% but increased the ^{9}C content.

These secondary beams were transmitted through the A1200 analyzing system [23] and delivered to the reaction product mass separator (RPMS) [24] which refined the velocity and momentum selections.

After leaving the RPMS, the secondary projectiles passed through two position-sensitive parallel-plate avalanche counters (PPAC's), 1.3 m apart, which measured their coordinates in the plane normal to the beam axis. The remaining telescope elements (see inset to Fig. 1) were 11 Si transmission detectors of 300 or 450 mm^2 active area; these served as both targets for the projectiles and detectors of the fragments. They were arranged so that each of five detectors of about 0.1 mm depletion depth (called D1 through D5) was followed by a 1 mm thick detector (E1 through E5). A 0.4 mm detector (E6) completed the telescope.

Projectiles accepted for analysis had appropriate time of flight to, and energy loss in, detector D1, and traveled within 5 mm of the telescope axis, as determined from the PPAC signals. Fragments were identified from scatter plots, such as Fig. 1, for the last two detectors E5 and E6. This plot shows both ^{7}Be fragments produced in the telescope and some straggling unreacted ^{8}B's. However, most unreacted ^{8}B's stopped in detector E5, since their average range [25] was 5.50 mm and the first ten detectors had a combined thickness of 5.65 mm. Most of the ^{7}Be fragments produced in or before detector E4 (but few from E5) reached detector E6, and therefore were easily distinguished from ^{8}B. Some fragments stopped in detector E6 but others were transmitted through it. Events in Fig. 1 below and to the left of the ^{7}Be's are expected to be primarily ^{3}He and ^{4}He. A few transmitted ^{6}Li fragments were identified in the D5 vs E5 spectrum; these events were removed from Fig. 1 and other analyzed spectra. However, we cannot estimate σ_{2p} for ^{8}B, since the most energetic (i.e., least ionizing) ^{6}Li fragments could not be resolved from the $Z=2$ group.

III. DATA ANALYSIS AND EXPERIMENTAL RESULTS

A. ^{8}B

Identified ^{8}B's, in a secondary beam of 5 mm radius, produced ^{7}Be fragments in the Si detector targets. These fragments were sorted into four production energy intervals; viz., the ranges of the projectile energies as they passed through detectors E1 through E4. This sorting required an additional two-dimensional identification gate—containing only those ^{7}Be events appearing in Fig. 1—which was applied to the energy spectra of the 0.1 mm detectors D2 through D5. These spectra, shown in Fig. 2, cleanly separate the ^{8}B's

which have not yet reacted from the ^{7}Be's already produced; the latter steadily increase downstream in the telescope while the former decrease. Since projectile selection is completed in detector D1, ^{7}Be events observed in detector D3 (for example) were produced in detectors E1, D2, and E2. The E detectors produce about ten times as many fragments as the D detectors because of their greater thickness; the few events between the ^{7}Be and ^{8}B groups in Fig. 2 are from fragmentation in the specified D detector. Since the ionization losses in the detectors vary with projectile energy, the horizontal scales in Fig. 2 are separately renormalized to align the ^{8}B peaks.

We determined σ_{1p} for each energy interval from the increase in the number of ^{7}Be fragments observed in the D detector following that interval's E detector over those in the one preceding it, the number of accepted projectiles, and the effective target thickness. For the highest-energy interval the tight energy gate set on detector D1 rejected all but a negligible number of fragments produced in it, so the target thickness was taken to be that of the E1 detector plus half that of D2. In the other three cases, the effective thickness was taken to be that of the corresponding E detector plus half of the adjacent D detectors. Corrections were made for reactions which attenuated the ^{8}B beam in the telescope, and for secondary reactions of the fragments which prevented their identification. These effects were calculated from the known reaction cross sections of ^{7}Be and ^{8}B in Si [3,17]; together they increased σ_{1p} by about 5%. Two roughly equal background estimates—about 2% of the total counts—were obtained from the event rate outside the peaks in Fig. 2, and from other D2 through D5 spectra gated on events from areas adjacent to the ^{7}Be events in Fig. 1. Experimental uncertainties were obtained by combining in quadrature the statistics of total and background events with an additional 5% estimate for the uncertainty in specifying the two-dimensional identification gate.

Further corrections to σ_{1p} would have been required if the momentum distribution of the fragments in the projectile rest frame had caused some fragments with large transverse momenta to scatter out of the telescope or others with large backward longitudinal momenta to have insufficient range to reach detector E6. Such losses are negligible if we assume a Gaussian distribution with a rest-frame full width at half maximum (FWHM) of 90 MeV/c, the value reported for ^{8}B on a Be target [11]. In contrast, a Lorentzian distribution [26] implies substantial corrections: e.g., 8% of the fragments produced in detector E1 are predicted to stop in detector E5. However, since none were observed to do so, we made no such corrections.

Our cross sections σ_{1p} for ^{8}B are shown in Fig. 3 and Table I. Their individual error bars overlap those of the other low-energy data [4,13] except for the points near 60 MeV/nucleon. However, as a group, the present data show the decrease of σ_{1p} with increasing energy predicted by theory, while the older data were consistent with energy independence.

B. ^{9}C

We first summarize Experiment 2, more fully described elsewhere [21], and then present the ^{9}C results obtained from

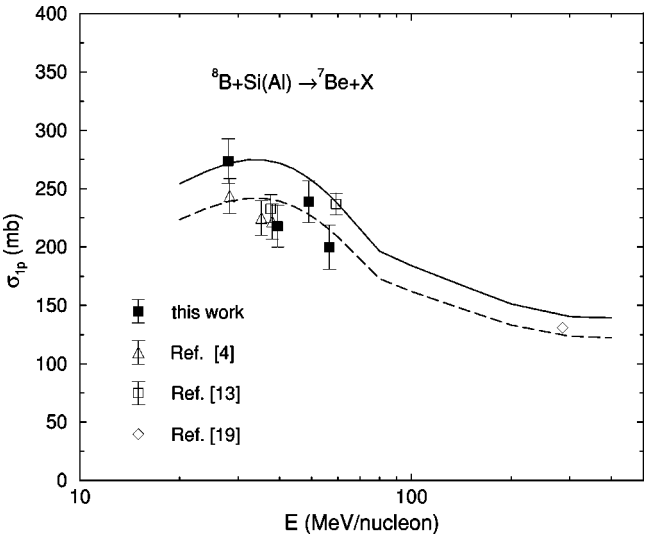

FIG. 3. Inclusive σ_{1p} for ^{8}B incident on Al or Si. Measurements are from the present work and Refs. [4,13,19]. The solid curve shows the prediction from Eq. (1) of Sec. IV; the dashed curve shows that prediction multiplied by the quenching factor R_s=0.88 which fits higher-energy data.

it. Two thin position-sensitive Si detectors, E1 and E2, selected a 55 MeV/nucleon ^{9}C secondary beam of 4 mm radius. The four detector targets, E3 through E6, were 0.5 mm thick. The ^{7}Be and ^{8}B fragments which they produced were identified in detectors E7 and E8, 0.5 mm and 5 mm thick respectively, using the empirical range-energy relationship $R=aE^p$ [17]. The energy loss spectra in detector E6 for these identified fragments are shown in Fig. 4. Each spectrum has a lower peak, caused mainly by fragments produced in detectors E3 through E5, and an upper peak (labeled "^{9}C") from fragments produced in E7 near its front face. The continuum between these peaks is from fragments produced in

TABLE I. Proton-removal cross sections for light nuclei on Si, averaged between specified energies. The theoretical predictions are described in Sec. IV.

Projectile, cross section	Fragment	Energy (MeV/nucleon)	Measurement (mb)	Prediction (mb)
^{8}B, σ_{1p}	^{7}Be	22–34	274±18	270
^{8}B, σ_{1p}	^{7}Be	34–45	218±19	271
^{8}B, σ_{1p}	^{7}Be	45–53	239±19	258
^{8}B, σ_{1p}	^{7}Be	53–60	200±18	244
^{8}B, σ_{1p}	^{7}Be	22–60	233±12	261
^{9}C, σ_{1p}	^{8}B	28–51	77±11	119
^{9}C, σ_{2p}	^{7}Be	28–51	198±16	
^{9}C, σ_{1p}	^{8}B	40–68	88±17	108
^{12}C, σ_{1p}	^{11}B	34–44	70±7	167
^{12}C, σ_{1p}	^{11}B	44–52	70±7	160
^{12}C, σ_{1p}	^{11}B	52–59	74±6	150
^{12}C, σ_{1p}	^{11}B	34–59	71±4	161

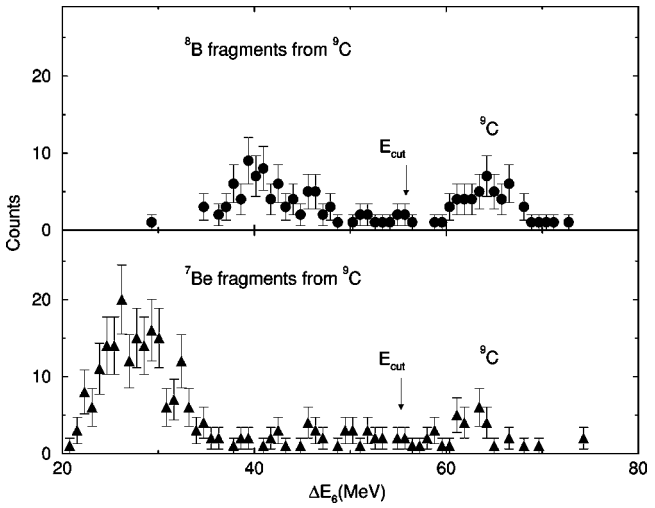

FIG. 4. Spectra of fragment energy losses in the final target detector (E6) of Experiment 2, from incident 55 MeV/nucleon ^{9}C. Most fragmentation events in the peaks marked "^{9}C" occur in detector E7 near its front face. Only events below the marked cutoff energy were counted; a model correction was made for events above it which occurred in E6 near its rear face.

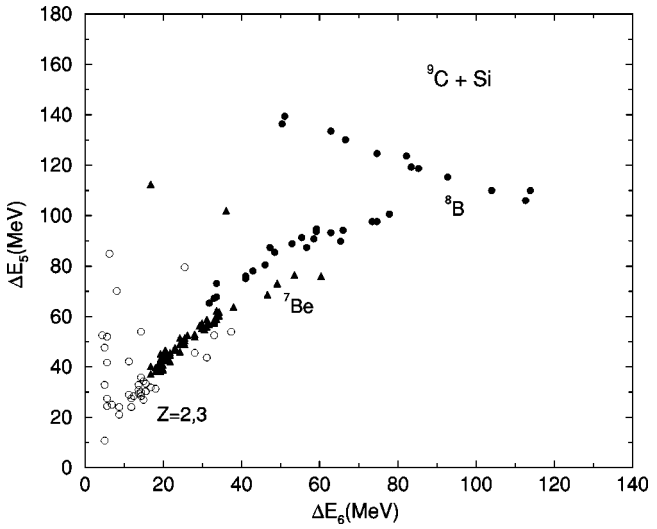

FIG. 5. Scatter plot of fragments from incident 69 MeV/nucleon ^{9}C identified in the last two detectors of Experiment 1. Each symbol represents one event; solid triangles are used for ^{7}Be and solid circles for ^{8}B. Unidentified events (empty circles) may include both particles with $Z \leqslant 3$ and large noise pulses. However most of the latter, with $E \leqslant 5$ MeV in either detector, are suppressed.

E6. To confine the production region to detectors E3 through E6, events above the cutoff energy shown in Fig. 4 were rejected, leaving 234 and 82 accepted ^{7}Be and ^{8}B events, respectively.

The measured proton-removal cross sections for Experiment 2 (projectile energies between 28 and 51 MeV/nucleon) are listed in Table I. These values include beam and fragment attenuation corrections of about 2%. For these corrections we assumed σ_R for ^{7}Be, ^{8}B, and ^{9}C on Si to be 1.6 ± 0.4 b; this range covers all measured σ_R's for light nuclei on Si at these energies [3,17]. Correcting for rejected fragments produced near the rear face of E6 (i.e., above the cutoff energy in Fig. 4) requires the rest-frame fragment momentum distribution. The Goldhaber model [27] gives a $1p$-FWHM of about 240 MeV/c for stable nuclei, and (for ^{9}C) a $2p$ FWHM which is $\sqrt{7/4}$ times as large. The $1p$ FWHM of ^{9}C was chosen to be 150 MeV/c since its S_p(1.3 MeV) is between those of ^{8}B(0.137 MeV) and normally bound nuclei ($\sim$8 MeV). This correction then added 9% and 5% to the $1p$ and $2p$ yields, respectively, while the other momentum-distribution corrections (for out-scattering and insufficient range) were negligible. Backgrounds of 8 (14) events for ^{7}Be(^{8}B) were subtracted after being observed in E6 spectra gated on particle-identification signals between and outside the peaks for ^{7}Be and ^{8}B fragments.

In Experiment 1, about 3×10^4 ^{9}C projectiles of 69 MeV/nucleon met the acceptance criteria for beam spread (5 mm radius), timing, and energy loss in detector D1. Only those fragments produced in detectors E1 through E3 and identified in the D2 through D4 energy spectra were counted, since many produced in E4 stopped before E6. The scatter plot for the two final detectors, Fig. 5, shows stopped and transmitted groups for both ^{7}Be and ^{8}B fragments, whose identities were confirmed from their signals in D4 and D5. The plot shows no long-range straggling ^{9}C's, as is expected since these projectiles have 0.15 mm less range in Si than the ^{8}B projectiles.

The value of σ_{1p} measured in Experiment 1 (projectile energies from 40 to 68 MeV/nucleon) is listed in Table I. This value of σ_{1p} includes a 9 ± 4 % correction for out-scattering, range distribution, and beam and fragment attenuation. There are 60 ^{7}Be events and 34 ^{8}B events identified in Fig. 5. Their ratio, 1.76 ± 0.38, is probably a lower limit since some ^{7}Be events appear to be lost among the $Z = 2,3$ events near the origin of Fig. 5. This count ratio is marginally consistent with the σ_{2p}/σ_{1p} ratio of 2.57 ± 0.42 found in Experiment 2. This cross section ratio is consistent with those found at 285 MeV/nucleon [19], which also suggest that the ratio is target dependent.

C. ^{12}C

The scatter plot for incident 59 MeV/nucleon ^{12}C was similar to that for ^{8}B shown in Fig. 1. A prominent ^{12}C straggling group was well resolved from a thin locus for stopped ^{11}B fragments, which were outnumbered by transmitted ^{11}B's. The latter were well resolved from Be events from $2p$ removal.

Yields of ^{11}B fragments from incident ^{12}C were obtained as were those of ^{7}Be from incident ^{8}B. Since the Goldhaber model [27] indicated momentum-distribution losses near 20% for fragments produced in E4, we report data only for detectors E1 through E3, for which these corrections were below 5%. Our measured σ_{1p} for ^{12}C on Si, presented in Table I, are comparable to those observed in ^{12}C + ^{12}C at higher energies [22].

IV. COMPARISON OF DATA WITH THEORETICAL MODELS

We calculate the single-particle cross sections σ_{sp} for the removal of a nucleon from the projectile, with unit spectro-

scopic factor, populating a given final state of the projectile residue. When only the residue is detected, this is an incoherent sum of the contributions from the elastic and inelastic breakup (stripping) mechanisms. These are calculated here using the spectator-core eikonal model [14,15]. Since the individual final states of the residue are also not observed in the experiments reported, the corresponding theoretical proton-removal cross section σ_{1p} is a sum,

$$\sigma_{1p}^{th} = \sum_{Ij\ell} S_{\text{c.m.}}(I^\pi, \ell j)\sigma_{sp}(S_p, I\ell j), \quad (1)$$

of contributions from reactions to all particle stable final states having a nonzero shell model spectroscopic strength. Here $S_{\text{c.m.}}(I^\pi, \ell j)$ are the spectroscopic factors for removal of a proton with single-particle quantum numbers n, ℓ, j, leaving the projectile residues in given final states I^π.

For the *p*-shell nuclei of interest, the spectroscopic factors in Eq. (1) are $S_{\text{c.m.}}(I^\pi, \ell j) = [A/(A-1)]S(I^\pi, \ell j)$. The $A/(A-1)$ factor has to be introduced to correct the bare (fixed center) shell model spectroscopic factors $S(I^\pi, \ell j)$ for center-of-mass (c.m.) effects in a light projectile of mass A [28,29]. The calculations of the single-particle cross sections $\sigma_{sp}(S_p, I\ell j)$ follow Eqs. (2) and (3) of Ref. [30], where S_p is the proton separation energy from the projectile ground state to a given final state I^π of its residue.

A. Calculations for ^{8}B

Our calculations for ^{8}B closely follow those of Ref. [22]. We adopt the shell model spectroscopic factors of Brown *et al.* [29] in which $S(\frac{3}{2}^-, 1\frac{3}{2}) = 0.97$ and $S(\frac{3}{2}^-, 1\frac{1}{2}) = 0.06$, both to the ^{7}Be ground state, and $S(\frac{1}{2}^-, 1\frac{3}{2}) = 0.22$ to the excited ^{7}Be$(1/2^-)$ state at 0.429 MeV. These values are consistent [22] with the recent direct measurement of this $I^\pi = 1/2^-$ component obtained at the Gesellschaft für Schwerionenforschung [8]. The proton separation energies to the ground and excited state are 0.1375 MeV and 0.5665 MeV, respectively. We assume that a central Woods-Saxon potential binds the protons in each single-particle configuration, with the potential depth adjusted to reproduce the required separation energy. The potential geometry was taken from Ref. [29], as used in Ref. [22], with radius parameter $r_0 = 1.254$ fm and diffuseness $a = 0.62$ fm, consistent with the Coulomb displacement energy for the $A = 7$ system. Thus the effective ^{7}Be ground- and $1/2^-$-state spectroscopic factors are $S_{\text{c.m.}}(3/2^-) = 8(0.97 + 0.06)/7 = 1.18$ and $S_{\text{c.m.}}(1/2^-) = 8(0.22)/7 = 0.25$, respectively.

The ^{7}Be-target elastic profile functions $S_7(b)$, and all subsequent residue-target profile functions, were calculated at all energies assuming the optical limit of the eikonal model [31]. Thus the assumed ^{7}Be and target one-body densities were (double) folded with an effective nucleon-nucleon (NN) interaction. This NN interaction was assumed to have zero range. The free NN cross sections were computed from the formulas of Charagi and Gupta [32]. Their real to imaginary part ratios were interpolated from the tabulation of Ray [33] for $E \geqslant 100$ MeV/nucleon and were set to the 100 MeV values for $E < 100$ MeV/nucleon. The ^{7}Be matter density was assumed to be Gaussian with a root mean squared (rms) radius of 2.31 fm [34]. The target (Si) density was assumed to be given by the global Fermi form parametrization of Negele [35], from which the rms matter radius is 3.165 fm. The calculated ^{7}Be-Si elastic profile functions are highly absorptive at all energies and there is very little sensitivity to these parameters in the calculations.

This optical limit approach is not appropriate, however, for the proton-target profile function $S_p(b)$ at the lowest energies we consider here. For all the lower-energy calculations, $E \leqslant 80$ MeV/nucleon, we used the proton-target profile functions calculated using the exact continued phases method [36], in which the exact partial wave S matrix was analytically continued for noninteger orbital angular momenta $\lambda = kb - 1/2$. These improved $S_p(b)$ were computed from the proton-target optical potential calculated using the midpoint local density approximation [37] and the Jeukenne, Lejeunne, and Mahaux (JLM) effective NN interaction [38]. In calculating this potential we included the required effective mass correction to the imaginary part **(**Eq. (29) of [38]**)** discussed in Refs. [39,40]. We used the conventional scale factors for the real and imaginary parts of the JLM optical potentials, $\lambda_V = 1.0$ and $\lambda_W = 0.8$, required to fit a body of elastic scattering and reaction cross section data [37] for light and medium mass targets. For energies above 80 MeV/nucleon we used the optical limit approximation for $S_p(b)$ using the same effective interactions as were discussed for the ^{7}Be - target system.

The predictions for projectile energies from 20 to 400 MeV/nucleon are presented in Fig. 3. Inclusive measurements at higher energies are generally smaller than the theoretical predictions for ^{8}B by a quenching factor $R_s = 0.88 \pm 0.04$ [22]. This factor, attributed to short-range, cluster, and other correlation effects [41], is thought to be close to unity since ^{8}B is primarily ^{7}Be$+p$ in nature. Most of the low-energy ^{8}B data are also well fitted when this factor is applied to the predictions of Eq. (2), as is shown by the dashed curve of Fig. 3.

For improved statistical accuracy we have averaged the measured σ_{1p} over all four energy ranges. The predicted energy-averaged cross section is then defined by [17]

$$\overline{\sigma_{1p}} = \int [\sigma_{1p}(E)/(dE/dx)]dE \Big/ \int [1/(dE/dx)]dE. \quad (2)$$

The weighting allows for the projectile's encountering progressively thinner target elements per unit energy loss as it slows down. Comparing the measured value, 233 ± 12 mb, with the prediction of 261 mb (see Table I) yields a quenching factor $R_s = 0.89 \pm 0.05$. This agrees very well with both the high-energy value 0.88 ± 0.05 [22] and also the value 0.86 ± 0.07 recently reported for ^{8}B$+^{12}$C at 76 MeV/nucleon [18].

B. Calculations for ^{9}C

The total spectroscopic strength for proton removal from ^{9}C to the 2^+ ^{8}B ground state is $S(2^+, 1) = 0.94$, with contribu-

tions of 0.93 and 0.01 from the $j^{\pi}=p_{3/2}$ and $p_{1/2}$ proton configurations, respectively [42]. Thus the effective ^{8}B ground-state spectroscopic factor is $S_{\mathrm{c.m.}}(2^{+},1)=9(0.94)/8=1.06$. The proton separation energy in this case is 1.296 MeV. The same central Woods-Saxon binding potential geometry was assumed as for the ^{8}B case [29]. Calculation of the ^{8}B-target elastic profile functions follow that for ^{7}Be, above, with an assumed ^{8}B rms matter radius of 2.38 fm. A radial mismatch factor $M=0.976$, discussed in Ref. [43], and which accounts for the difference of the last proton's orbital in ^{8}B from that occupied in ^{9}C, was also included as a scaling factor on the calculated cross sections; see also Ref. [18]. All calculations use the JLM effective interaction for the proton-target system.

Our σ_{1p} values measured in the two experiments are given in Table I. Comparing them with theoretical predictions yields $R_s=0.82\pm0.16$ for Experiment 1 (40–68 MeV/nucleon) and $R_s=0.65\pm0.09$ for Experiment 2 (28–51 MeV/nucleon). The weighted average of these values is 0.69 ± 0.08, which marginally agrees with the value 0.82 ± 0.06 recently reported for 78 MeV/nucleon ^{9}C on a carbon target [18]. More data on other targets would be needed to establish a target dependence, though it is interesting that the ratio of σ_{2p} to σ_{1p} seems to fall with increasing target mass [19].

C. Calculations for ^{12}C

From the point of view of structure input, our calculations for ^{12}C follow closely those of Ref. [22]. As discussed there, the $p_{3/2}$-subshell spectroscopic sum rule (of 4) is essentially exhausted for proton removal to just three bound final states of ^{11}B, the $3/2^{-}$ ground state with $S\left(\frac{3}{2}^{-},1\right)=3.16$, the $1/2^{-}$(2.125 MeV) state with $S\left(\frac{1}{2}^{-},1\right)=0.58$, and the $3/2^{-}$(5.020 MeV) state with $S\left(\frac{3}{2}^{-},1\right)=0.19$. The ground-state proton separation energy in this case is large, 15.95 MeV, and the binding potential geometry assumed was $r_0=1.310$ fm and $a=0.55$ fm, as in Ref. [22].

The present reaction calculations differ from those of Ref. [22] in three respects. The first is, as for ^{8}B and ^{9}C, at these lower energies we use the JLM effective interaction for the proton-target system. The second is that, because of the higher Z target and the lower incident energy, we include the correction of Vitturi and Zardi [44] to the projectile's impact parameter, $b'=(\eta+\sqrt{\eta^2+k^2b^2})/k$, to take account of the small Coulomb deflection from the eikonal straight line paths. This pushes the projectile to larger distances of closest approach and so reduces the cross section slightly; but this is everywhere less than 4%.

The third and more important consideration is the assumed rms matter radius of the ^{11}B core or residue. It was found that, at these lower energies, and due to the less absorptive nature of the JLM proton-target interaction, our calculated proton-removal cross sections show much greater sensitivity to the assumed core matter radius. In Ref. [22] the value of 2.11 fm was assumed, the mean of the values 2.09 fm (^{11}B) and 2.12 fm (^{11}C) deduced from interaction cross section analyses [34]. However, this value is anomalously small when compared to the neighboring boron isotopes, 2.20 fm (^{10}B) and 2.39 fm (^{12}B), with mean 2.30 fm. Also, structurally, there is no apparent basis for this reduced value for ^{11}B. The SKX Skyrme-Hartree-Fock densities of Brown *et al.* [45] agree very well with the systematics of both interaction cross section and charge radii measurements, and suggest an rms matter radius of 2.33 ± 0.03 fm for the ^{11}B and ^{11}C isobars [46]. We use this value for our comparisons with the data in Table I. For information, if we assumed a ^{11}B rms radius of 2.11 fm and also neglected the Coulomb impact parameter correction, the ^{12}C entries in Table I would be 213, 200, 186, and 202 mb, respectively.

Our final calculations and the data, from 34 to 59 MeV/nucleon, are presented in Table I. The experimental data and theoretical predictions, averaged over this complete energy range, yield an R_s of 0.44 ± 0.03. The higher-energy value of R_s [22], deduced from data above 1 GeV/nucleon, was 0.53 ± 0.02 for a ^{12}C target. Additional data at other energies and with lower uncertainties would allow for a more rigorous comparison in this very important test case.

V. CONCLUSIONS

The method of Experiment 1, using alternating thin and thick Si detectors, was designed for measuring reaction cross sections σ_R on a Si target. However, we have shown that it is also effective for measuring the energy dependence of charge-removal cross sections. In particular, our measurements show significant energy dependence for σ_{1p} of the weakly bound nucleus ^{8}B but not the strongly bound ^{12}C.

Our shell model calculations, with eikonal reaction theory, produce results for σ_{1p} of the weakly bound nuclei ^{8}B and ^{9}C, consistent with those at higher energies. They require quenching factors R_s close to unity at all energies. The ^{12}C cross section data of this work are significantly quenched relative to the values predicted using eikonal reaction theory and shell model spectroscopy, as was also found in the interpretation of higher-energy data [22]. Sensitivity to the assumed core matter radius was found in this well-bound-proton, lower-energy regime. Further experimental studies, particularly in the region from 60 to 300 MeV/nucleon, are now needed for all these systems to provide a more definitive test of the theory and for delineating the source of the observed quenching.

The very large σ_{2p} observed for ^{9}C, comparable to σ_{1p} for ^{8}B, suggests consideration of this nucleus as a two-proton-halo candidate. Further measurements of its σ_{xp} on other targets, as well as of σ_R and the fragment momentum distributions, will provide more insight into the structure of this nucleus.

ACKNOWLEDGMENTS

We thank Peter Schwandt, Brad Sherrill, Christine Carpenter, Jon Kruse, Ashok Muthukrishnan, and Jing Wang for assistance with the measurements reported here. We also thank Alex Brown for providing clarification of the

Skyrme-Hartree-Fock matter radii for the mass 11 isobars and James Kolata for his comments on the sub-Coulomb ^{8}B reaction data. Financial support was provided by the Department of Energy under Grant No. DE-FG02-97ER41042 (TUNL), the National Science Foundation under NSF Grant Nos. PHY-0110253 (NSCL), PHY-0100102 (UM-Ann Arbor), and PHY-9971836 (UM-Dearborn), and the United Kingdom Engineering and Physical Sciences Research Council under Grant No. GR/M82141 (Surrey).

[1] T. Minamisono *et al.*, Phys. Rev. Lett. **69**, 2058 (1992).
[2] V. Guimaraes *et al.*, Phys. Rev. Lett. **84**, 1862 (2000).
[3] R. E. Warner *et al.*, Phys. Rev. C **52**, R1166 (1995).
[4] F. Negoita *et al.*, Phys. Rev. C **54**, 1787 (1996).
[5] W. Schwab *et al.*, Z. Phys. A **350**, 283 (1995).
[6] J. J. Kolata *et al.*, Phys. Rev. C **63**, 024616 (2001).
[7] F. Carstoiu, L. Trache, C. A. Gagliardi, R. E. Tribble, and A. M. Mukhamedzhanov, Phys. Rev. C **63**, 054310 (2001).
[8] D. Cortina-Gil *et al.*, Phys. Lett. B **529**, 36 (2002).
[9] M. M. Obuti, T. Kobayashi, D. Hirata, Y. Ogawa, A. Ozawa, K. Sugimoto, I. Tanihata, D. Olson, W. Christie, and H. Wieman, Nucl. Phys. **A609**, 74 (1996).
[10] A. Csótó, Phys. Lett. B **315**, 24 (1993).
[11] J. H. Kelley *et al.*, Phys. Rev. Lett. **77**, 5020 (1996).
[12] R. E. Warner, I. J. Thompson, and J. A. Tostevin, Phys. Rev. C **65**, 044617 (2002).
[13] M. Fukuda *et al.*, Nucl. Phys. **A656**, 209 (1999).
[14] J. A. Tostevin, Nucl. Phys. **A682**, 320c (2001).
[15] K. Hencken, G. F. Bertsch, and H. Esbenseen, Phys. Rev. C **54**, 3043 (1996)
[16] A. Ozawa *et al.*, Phys. Lett. B **334**, 18 (1994).
[17] R. E. Warner *et al.*, Phys. Rev. C **64**, 044611 (2001).
[18] J. Enders *et al.*, Phys. Rev. C **67**, 064301 (2003).
[19] B. Blank, C. Marchand, M. S. Pravlikoff, T. Baumann, F. Boué, H. Geissel, M. Hellström, N. Iwasa, W. Schwab, K. Sümmerer, and M. Gai, Nucl. Phys. **A624**, 242 (1997).
[20] L. Trache, F. Carstoiu, A. M. Mukhamedzhanov, and R. J. Tribble, Phys. Rev. C **66**, 035801 (2002).
[21] R. E. Warner *et al.*, Nucl. Phys. **A635**, 292 (1998).
[22] B. A. Brown, P. G. Hansen, B. M. Sherrill, and J. A. Tostevin, Phys. Rev. C **65**, 061601(R) (2002).
[23] B. M. Sherrill, D. J. Morrissey, J. A. Nolen, Jr., N. A. Orr, and J. A. Winger, Nucl. Instrum. Methods Phys. Res. B **70**, 298 (1992).
[24] L. H. Harwood and J. A. Nolen, Jr., Nucl. Instrum. Methods Phys. Res. **186**, 435 (1981).
[25] J. P. Biersack and J. F. Ziegler, computer code SRIM, Version 91.14 (IBM Corp., Yorktown, USA, 1992).
[26] J. H. Kelley, S. M. Austin, D. Bazin, T. Kubo, and B. M. Sherrill, Nucl. Instrum. Methods Phys. Res. A **386**, 492 (1997).
[27] A. S. Goldhaber, Phys. Lett. **53B**, 306 (1974).
[28] A. E. L. Dieperink and T. de Forest, Phys. Rev. C **10**, 543 (1974).
[29] B. A. Brown, A. Csótó, and R. Sherr, Nucl. Phys. **A597**, 66 (1996).
[30] V. Maddalena *et al.*, Phys. Rev. C **63**, 024613 (2001).
[31] J. S. Al-Khalili, J. A. Tostevin, and I. J. Thompson, Phys. Rev. C **54**, 1843 (1996).
[32] S. K. Charagi and S. K. Gupta, Phys. Rev. C **41**, 1610 (1990).
[33] L. Ray, Phys. Rev. C **20**, 1857 (1979).
[34] A. Ozawa, T. Suzuki, and I. Tanihata, Nucl. Phys. **A693**, 32 (2001).
[35] J. W. Negele, Phys. Rev. C **1**, 1260 (1970).
[36] J. M. Brooke, J. S. Al-Khalili, and J. A. Tostevin, Phys. Rev. C **59**, 1560 (1999).
[37] J. S. Petler, M. S. Islam, R. W. Finlay, and F. S. Dietrich, Phys. Rev. C **32**, 673 (1985).
[38] J.-P. Jeukenne, A. Lejeunne, and C. Mahaux, Phys. Rev. C **16**, 80 (1977).
[39] J. W. Negele and K. Yazaki, Phys. Rev. Lett. **47**, 71 (1981).
[40] S. Fantoni, B. L. Friman, and V. Pandharipande, Phys. Lett. **104B**, 89 (1981).
[41] V. R. Pandharipande, I. Sick, and P. K. A. deWitt Huberts, Rev. Mod. Phys. **69**, 981 (1997).
[42] B. A. Brown, Prog. Part. Nucl. Phys. **47**, 517 (2001).
[43] A. Navin *et al.*, Phys. Rev. Lett. **85**, 266 (2000).
[44] A. Vitturi and F. Zardi, Phys. Rev. C **36**, 1404 (1987).
[45] B. A. Brown, S. Typel, and W. A. Richter, Phys. Rev. C **65**, 014612 (2001).
[46] B. A. Brown (private communication).